Journal of Molecular Liquids 379 (2023) 121654

Contents lists available at ScienceDirect

Journal of Molecular Liquids

journal homepage: www.elsevier.com/locate/molliq

Mixed micelles and gels of a hydrophilic poloxamine (Tetronic 1307) and miltefosine: Structural characterization by small-angle neutron scattering and in vitro evaluation for the treatment of leishmaniasis

Zeinab Dirany [a], Rima El-Dirany [b,c], Gregory N. Smith [d], Paul Nguewa [b,*], Gustavo González-Gaitano [a,*]

[a] Department of Chemistry, School of Sciences, University of Navarra, 31080 Pamplona, Spain
[b] ISTUN Institute of Tropical Health, Department of Microbiology and Parasitology, University of Navarra, Irunlarrea 1, 31008 Pamplona, Spain
[c] Laboratory of Molecular Biology and Cancer Immunology, Faculty of Sciences I, Lebanese University, Hadath 1003, Lebanon
[d] ISIS Neutron Muon Source, Science and Technology Facilities Council, Rutherford Appleton Laboratory, Didcot OX11 0QX, United Kingdom

ARTICLE INFO

Article history:
Received 26 January 2023
Revised 6 March 2023
Accepted 13 March 2023
Available online 16 March 2023

ABSTRACT

Hypothesis/background: Tetronic® is a family of four-armed amphiphilic block copolymers of polyethylene oxide (PEO) and polypropylene oxide (PPO) that self-aggregate to form micelles and hydrogels. Due to their temperature and pH-responsiveness, they are emerging as smart nanomaterials in the area of drug delivery. Here we propose the use of Tetronic 1307 (T1307) as a nanocarrier of miltefosine (MF), a zwitterionic alkylphospholipid highly active against leishmaniasis, one of the most threating neglected tropical diseases. Given the amphiphilic nature of the drug, both surfactants can combine to form mixed micelles, reducing the cytotoxicity of MF by lowering its dose and improving its internalization, hence its antileishmanial effect.

Experiments: The structure of the T1307 micelles, MF micelles, mixed micelles and hydrogels, formed in buffered solution (pH = 7.4) at different concentrations has been investigated in-depth by a combination of small-angle neutron scattering (SANS), dynamic light scattering (DLS), fluorescence spectroscopy and nuclear magnetic resonance methods (1D, 2D NOESY, and diffusion NMR). The cytotoxicity of the aggregates in macrophages has been assessed, as well as the antileishmanial activity in both *Leishmania major* promastigotes and amastigotes.

Findings: T1307 and MF combine into mixed aggregates over a wide range of temperatures and compositions, forming ellipsoidal core–shell mixed micelles. The shell is highly hydrated and comprises most of the PEO blocks, while the hydrophobic core contains the PO blocks and the MF along with a fraction of EO and water molecules, depending on the molar ratio in the mixture. The combination with T1307 amplified the leishmanicidal activity of the drug against both forms of the parasite and dramatically reduced drug cytotoxicity. T1307 micelles also showed a considerable leishmanicidal activity without exhibiting macrophage toxicity. These results support the use of T1307 as a MF carrier for the treatment of human and animal leishmaniasis, in its different clinical forms.

1. Introduction

Polymeric micelles (PMs) are nanoscopic structures of 5–100 nm, formed through the self-assembly of amphiphilic block copolymers [1]. In their simplest configuration, PMs are structured in a hydrophobic core and a hydrophilic shell and can adopt different shapes such as spheres, ellipsoids, or worm-like micelles [2]. Due to their structure, loading capacity, easy preparation, and low toxicity, PMs have been extensively investigated as nanocarriers for drug delivery via different administration routes [3–6]. A promising type of PMs is based on poloxamines, also known as Tetronic®, X-shaped copolymers formed by four arms of polyethylene oxide (PEO) and polypropylene oxide (PPO) blocks connected by an ethylene diamine spacer. They are commercially available in a variety of molecular weights, EO/PO ratios, and block configuration, which strongly determine their self-aggregation capacity, sol–gel transition, and temperature response [7]. The phase transitions also depend on the degree of protonation of the diamine central group, which confer pH-sensitivity to the polymer, as an advantage over their linear counterparts, Pluronic® family [8]. Tetronic sur-

* Corresponding authors.
E-mail addresses: panguewa@unav.es (P. Nguewa), gaitano@unav.es (G. González-Gaitano).

https://doi.org/10.1016/j.molliq.2023.121654
0167-7322/

factants have been also studied for their ability to form polyrotaxanes by their combination with macrocycles, leading to the formation of supramolecular self-assemblies with applications in different fields, mainly in tissue engineering and drug delivery [9,10]. All these features make poloxamines versatile for biomedical applications, capable of solubilizing hydrophobic drugs in both micelle and gels to produce their controlled release, improving the permeability through biological barriers, increasing the bioavailability, and reducing the potential side effects [11–15].

In this work, we have focused on the hydrophilic poloxamine Tetronic 1307 (T1307) as a nanocarrier for miltefosine (MF), an alkylphospholipid agent currently used in clinic for the treatment of leishmaniasis, a neglected tropical disease with high morbidity and mortality rates. Leishmaniasis, in its different clinical forms (cutaneous, mucocutaneous, and visceral) is caused by parasites belonging to the genus *Leishmania* and transmitted to humans and animals by the bite of phlebotomine sandflies [16]. Initially developed as an anticancer agent, MF has demonstrated a potent antileishmanial activity and has been used for several decades to treat the disease [17]. However, MF presents limitations, like dose-limiting gastrointestinal adverse effects, relatively high cost, teratogenicity [18,19], and increasing relapse rate after treatment [20,21]. Moreover, drug resistance to MF has been also described, likely due to its long elimination half-life [22]. The mechanisms of resistance of MF seem to be related to deficiency in the drug internalization [19]. These drawbacks could be overcome by an adequate reformulation by using nanocarriers that can deliver the drug more efficiently into the macrophages using lower amounts of MF, thus reducing the side effects and controlling the drug resistance [23]. As an example, a formulation of MF with the linear block copolymer Pluronic F127 has been described, which proved to reduce the haemolytic potential of the drug while keeping the cytotoxicity in cancer cell lines [24].

Generally, mixed micelles formed by more than one type of amphiphile are capable to optimize the properties of the micellar systems, such as the thermodynamic stability, the size of the particles, toxicity, and drug permeability [1,25]. Given the amphiphilic nature of both carrier and drug, the formation of mixed micelles to a large extent is expected. In the last decades, several drug candidates and promising therapeutic targets have been studied to discover new or more efficient leishmanicidal medicines [16,26–32]. Recent work in our group has reported the encapsulation of MF in water using PEO-based surfactants (D-α-tocopheryl polyethylene glycol succinate and other poloxamines), proving that MF is largely incorporated into the PMs to form mixed aggregates in a wide range of temperatures and concentrations [29].

Within this context, the purpose of this work was to develop a drug delivery system to improve the biological properties of MF through its combination with T1307, which entails the in-depth structural study of the aggregates, the conditions under which both molecules combine and the *in-vitro* evaluation of the formulations. The self-aggregation of T1307 has been fully characterised by mimicking the physiological conditions in both the diluted and concentrated regimes (gels), as well as of MF-T1307 mixed micelles and gels. A combination of scattering (SANS, DLS) and spectroscopic methods (1D-NMR, NOESY, DOSY) has been used to this purpose. Then, cytotoxicity assays were performed in murine macrophages and the antiparasitic activity studied in *Leishmania major* parasites, on both promastigote and amastigote forms, since one of the goals of this work is the development of an improved, safe and active formulation of MF for leishmaniasis treatment. Our results show that the combination of the drug with T1307 can achieve this goal, enhancing the antileishmanial activity of MF and inhibiting its cytotoxic effect.

2. Materials and methods

2.1. Materials

Tetronic 1307 (T1307) was a gift from BASF. The reported composition per arm is 72 EO and 23 PO (average molar mass 18,000 g·mol^{-1}). Unless otherwise stated, the concentrations are expressed in mass percentage. Miltefosine (MF, molar mass 407.57 g·mol^{-1}) was purchased from Avanti® Polar-Lipids-Sigma Aldrich and Glentham Life Sciences.

2.2. Phase behavior of T1307

Concentrated solutions of T1307 (15% to 30%) were prepared in water, phosphate-buffer (PB, pH 7.4) and D_2O. 1.5 ml of solution were introduced in cylindrical glass tubes which were then placed in a dry-bath incubator (Thermo scientific). The temperature was varied in 5 ºC increments from 15 to 70 °C and the physical state of the sample noted after 5 mins of equilibration at each temperature.

2.3. Dynamic light scattering (DLS)

Intensity size distributions were obtained with a Protein Solutions DynaPro photon correlation spectrometer with a laser wavelength of 822 nm. The temperature was controlled by the built-in Peltier unit. The experiments were carried out for solutions of T1307 and mixtures with MF in different solvents (water, PBS, D_2O) as a function of the temperature, from 15 to 60 °C in 5 °C increments, in semi-micro glass cells. Prior to the measurements, the samples were filtered using syringe filters of either 0.22 μm (PVDF Millex) or 0.02 μm (Whatman, inorganic membrane) pore size. The temperature dependence of the viscosities and refractive indices of the different solvents [33,34] were considered for the calculation of the apparent hydrodynamic sizes, R_h, which were deduced from the Stokes-Einstein equation as

$$R_h = k_B T / 6\pi\eta D$$

where D is the diffusion coefficient of the particle, k_B is the Boltzmann constant, η is the viscosity of the solvent and T the absolute temperature. The particle size distributions were obtained from the analysis of the autocorrelation functions using the default regularization algorithm, implemented in the DynaLS 6.0 software.

2.4. Critical micelle concentration (CMC) determination

Pyrene fluorescence emission was used to determine the critical micelle concentration (CMC) of T1307, MF and their combinations. The emission spectra were obtained with a FLS920 spectrofluorometer (Edinburgh Instruments). The surfactants were dissolved in 10^{-6} M stock solutions of pyrene (PBS or water) in order to keep constant the concentration of the probe along the titration, which was carried out directly in the measuring cell (quartz cuvettes of 10 mm path-length) with a micropipette under constant stirring. Samples were excited at 336 nm and the spectra recorded between 345 and 450 nm. The ratio of the emission of III (384 nm) to I (373 nm) vibronic bands was used to detect the polarity changes of the probe in the hydrophobic environment of the micelles, and the CMC determined by plotting the I3/I1 ratios versus the surfactant concentration as the value at which the first derivative remains constant [35]. Measurements were performed at different temperatures (20, 30, 37 and 45 °C, 0.1 °C accuracy) by recirculating water from an external bath.

2.5. Nuclear magnetic resonance spectroscopy (NMR)

1D, 2D-NOESY, and 2D-DOSY NMR proton spectra were recorded in a Bruker Avance Neo 400 spectrometer (400 MHz). The spectrometer default pulse sequences were used for recording the 1D and 2D-NOESY spectra. For the diffusion experiments, bipolar pulse longitudinal eddy current delay (BPLED) pulse sequences were used (ledbpgp2s1d and ledbgpg2s). 1D-proton spectra were recorded first for each gradient applied and the attenuation of the selected resonances of each spectrum analysed by integration. The separation of the gradients and their duration (Δ and δ, respectively) were optimized to ensure the complete exponential decay of the signal with the gradient. 2D Diffusion Ordered Spectroscopy representation (DOSY), with the NMR spectra on the x-axis and the diffusion coefficient (D) on the y-axis, was obtained with Mnova software (Mestrelab research), by using the Bayesian transformation of the collected spectra. The hydrodynamic radii were obtained from the diffusion coefficients through the Stokes-Einstein equation, by introducing the corresponding solvent viscosities. All samples were prepared by dissolving the required amounts of solutes in D_2O or PB (KH_2PO_4 and Na_2HPO_4 in deuterium oxide, Aldrich, deuterium content > 99.96%).

2.6. Small angle neutron scattering (SANS)

SANS measurements were performed on the Larmor instrument at the ISIS Neutron and Muon Source (Rutherford Appleton Laboratory, UK) [36]. In its SANS configuration, Larmor is a fixed-configuration time-of-flight, pinhole SANS instrument with a sample-to-detector distance 4 m. The usable wavelength (λ) range on T2 at ISIS is $0.9 < \lambda < 13.5$ Å, which gives a maximum q range of $0.004 < q < 0.7$ Å^{-1}, where q is the magnitude of the momentum transfer vector, $q = 4\pi \sin(\theta)/\lambda$. Two different wavelength ranges were used for data processing: a broad range ($0.9 < \lambda < 13.5$ Å) for dilute samples to study the widest range of length scales and a reduced range ($6.0 < \lambda < 13.5$ Å) for gels to improve resolution of peaks. Samples were loaded into either 1 or 2 mm path-length cylindrical quartz cells, which were placed in Larmor's temperature-controlled sample changer, and illuminated by an 11×11 mm^2 beam for the measurements. Data were converted from raw data to reduced data of scattering intensity (equivalently the scattering cross section per unit volume, $d\Sigma/d\Omega(q)$) as a function of q by correcting for detector efficiency and sample transmission using the instrument-specific software Mantid [37,38]. The raw data were placed on an absolute scale (cm^{-1}) by measuring the scattering of a mixture of hydrogenous and deuterated polystyrene with known radius of gyration and scattering cross section [39]. The scattering from the solvent was measured, processed the same way, and subtracted from the sample data. SANS curves were fitted using SasView 5.0.5 software [40]. The information on the models used and fitting procedures was described extensively in the Results and Discussion section and in the Supporting Information.

2.7. Biological evaluation of the formulations

(i) Cells and culture conditions

Leishmania major promastigotes (Lv39c5) were grown at 26 °C in M199 medium supplemented with 25 mM HEPES (pH 7.2), 0.1 mM adenine, 0.0005% (wt/vol) hemin, 2 mg/ml biopterin, 0.0001% (wt/ vol) biotin, 10% (vol/vol) heat-inactivated foetal bovine serum (FBS), and an antibiotic cocktail (50 U/ml penicillin, 50 mg/ml streptomycin). To maintain their infectivity, *Leishmania* cells were isolated from infected BALB/c mouse spleen and parasites were maintained in culture for no more than five passages. Murine bone marrow-derived macrophages (BMDMs) were obtained as previously described [16,41]. All the procedures involving animals were approved by the Animal Care Ethics Commission of the University of Navarra [approval number: E5-16 (068-15E1) 25 February 2016].

(ii) Cytotoxicity in macrophages

The cytotoxicity of T1307, MF, and the mixtures was studied in murine macrophages using the 3-[4,5-dimethylthiazol-2-yl]-2,5-diphenyltetrazolium bromide (MTT) colorimetric assay (Sigma, St. Louis, MO, USA). MTT solutions were prepared at 5 mg/ml in phosphate-buffered saline (PBS), filtered and maintained at –20 °C until use. Briefly, 5×10^4 cells per well were seeded in 96-well plates and allowed to adhere for 24 h at 37 °C in a 5% CO_2 humidified atmosphere. The culture medium was replaced by fresh medium with increasing concentrations of the compounds and, after 48 h of incubation, 20 µl/well of MTT were added and the plates were incubated 4 h under the same conditions. Then, the medium was removed and 100 µl of dimethyl sulfoxide (DMSO) was added to each well to dissolve the formazan crystals. The optical density (OD) was measured in a Multiskan EX microplate photometer plate reader at 540 nm, and the cell viability was calculated with respect to untreated cells. The results were expressed as means (±standard deviation, SD) from two independent experiments.

(iii) Activity against promastigotes

Exponentially growing cells (2×10^6 *L. major* promastigotes/ml) were seeded in 96-well plates (100 µl per well) with increasing concentrations of the treatments, which were diluted in M199 culture medium. After 48 h of incubation, MTT assays were performed as previously described [29]. The half-maximal inhibitory concentration (IC_{50}) was calculated. The IC_{50} represents the concentration required for 50% growth inhibition of treated cells with respect to untreated cells (controls) and was obtained by fitting a sigmoidal E_{max} model to dose–response curves.

(iv) Intracellular amastigote assays

Murine macrophages were seeded in 8-well culture chamber slides (Lab-Tek^{TM}, BD Bioscience) at a density of 5×10^4 cells per well in DMEM medium and allowed to adhere overnight at 37 °C in a 5% CO_2 incubator. To perform the infection assay, metacyclic promastigotes were isolated by the peanut agglutinin (PNA) method and used to infect the macrophages at a macrophage/parasite ratio 1/10. The plates were incubated for 24 h under the same conditions until promastigotes were phagocytosed by the macrophages. Afterwards, wells were washed with PBS to remove the extracellular promastigotes, and plates were incubated with fresh medium supplemented with increasing concentrations of the treatments. 48 h later, cells were washed with PBS, fixed with ice-cold methanol for 5 min, and stained with Giemsa stain. To determine the parasite burden, high resolution images of Lab-Teks were captured using a transmitted light optical microscope (Leica). The images were analysed using Fiji software [42], measuring the number distributions of amastigotes and macrophages according to their different sizes with the implemented algorithm Analyze Particles. The number of amastigotes per infected macrophage was then determined by dividing the total number of amastigotes by the number of infected macrophages (at least 100 macrophages). Two independent experiments were performed, with duplicates.

(v) Statistics

The statistical analysis was carried out using *GraphPad Prism* version 5.0. Two-tailed unpaired *t*-test was used for the comparison between two groups. The data were presented as mean ± SD. P-Values < 0.05 (*), <0.01 (**), <0.001 (***) were considered significant.

3. Results and Discussion

3.1. Aggregation and structure of MF-loaded polymeric micelles

3.1.1. Micellization of T1307 in buffered medium

The self-aggregation of T1307 in water as a function of the temperature and concentration, as well as the effect of the pH has been described in a previous work [43]. Under very acidic conditions, the unimers are fully protonated, hindering the micellization and the formation of gels. At physiological pH, according to the pKa values reported for this surfactant (4.6 and 7.8, [7]), 72 % of unimers are in their monoprotonated form, which can modify extent of the formation of aggregates [44] and, therefore, their structure and drug-loading capacity. Fig. 1a shows the intensity size distribution obtained from DLS of 1% T1307 at different temperatures in PB. At 15 °C and 25 °C, only unimers (3.2 nm in hydrodynamic radius, R_h) are present and, above 30 °C, the self-aggregation starts (additional peak at 9 nm). At 35 °C, the bimodal distribution coalesces and the micelles, evidenced in a broad peak, are the predominant forms. As the temperature increases, the distribution becomes narrower, with a slight reduction in the micelle size (8.7 nm at 55 °C). A similar pattern (micellization and further narrowing of the micelles distribution) can be observed at higher surfactant concentration (Fig. S1). The tendency of T1307 to self-aggregate increases in PB compared to water or D_2O, as shown in Fig. 2. For 1% in PB at 35 °C only micelles can be detected, while in water and D_2O the distribution is still bimodal, indicating that the fraction of non-micellized surfactant must be significant at this temperature. In addition, the micelles size decreases in the order PBS > H_2O > D_2O. In general, in solutions of ionic surfactants, the presence of salts favours the micellization, reducing the critical micelle concentration (CMC) and increasing the aggregation number [45]. Given the non-ionic character of T1307, the effect is much reduced but still noticeable, as reported for Tetronic 904 [46]. Regarding the isotopic substitution, it is accepted that D_2O forms stronger hydrogen bonds than H_2O, which affects the physical and chemical properties of solutes. Since the hydrophobic effect is based on the structuration of solvent molecules around the solute, with the accompanying changes in enthalpy and entropy of the system, shifts in the phase diagram of a surfactant as well as changes in the shape of the aggregates are expected [47,48]. In this case, D_2O favours to some extent the aggregation of the poloxamine compared to water (Figs. 2 and 7), as observed with other surfactants.

The determination of the critical concentration by fluorescence is shown in Fig. S2, in which the ratio of the intensities between the III and I pyrene emission bands is plotted as a function of the surfactant concentration, in PBS and water, at different temperatures. The micellization occurs in a rather broad concentration interval, as per usual in polymeric surfactants, and the CMC has been taken as the value at which the first derivative of the I3/I1 ratio remains constant, resulting in 0.08% in both solvents at 37 °C and 45 °C. At lower temperatures, the copolymer is still in its unimer form in both solvents, the smooth increase in intensity most likely due to interactions of the probe with the hydrophobic PPO moiety of the Tetronic. On the other hand, by using DLS, micelles can be detected at 0.05% (the lowest concentration tested) and 37 °C in PB (Fig. 1b). The differences in the CMC values from fluorescence and DLS can be ascribed to the distinct physical principles on which both methods are based, the latter being more sensitive to detecting aggregates in an early stage of formation.

In-depth information on the internal structure of the micelles has been obtained through SANS experiments. Fig. 3a shows the scattering curves for 1% T1307 at different temperatures. At 25 °C, the surfactant is in the form of unimers and the data have been fitted to a Gaussian four-arm star-polymer model. The radius of gyration is 44 Å, indicating a certain expansion of the copolymer in PB compared to water (32 Å and 42.4 Å at 20 °C and 30 °C,

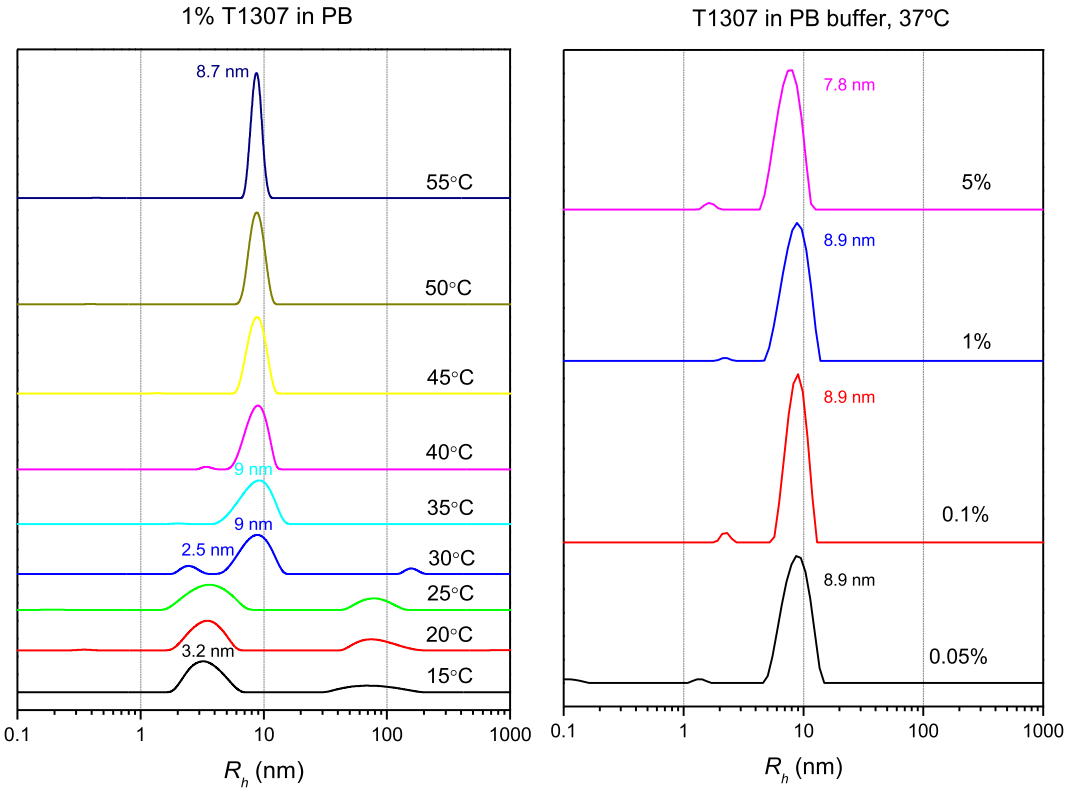

Fig. 1. (A) DLS size distributions of 1%T1307 in PB buffer (pH = 7.4) as a function of the temperature. (B) Size distributions as a function of the concentration at 37 °C.

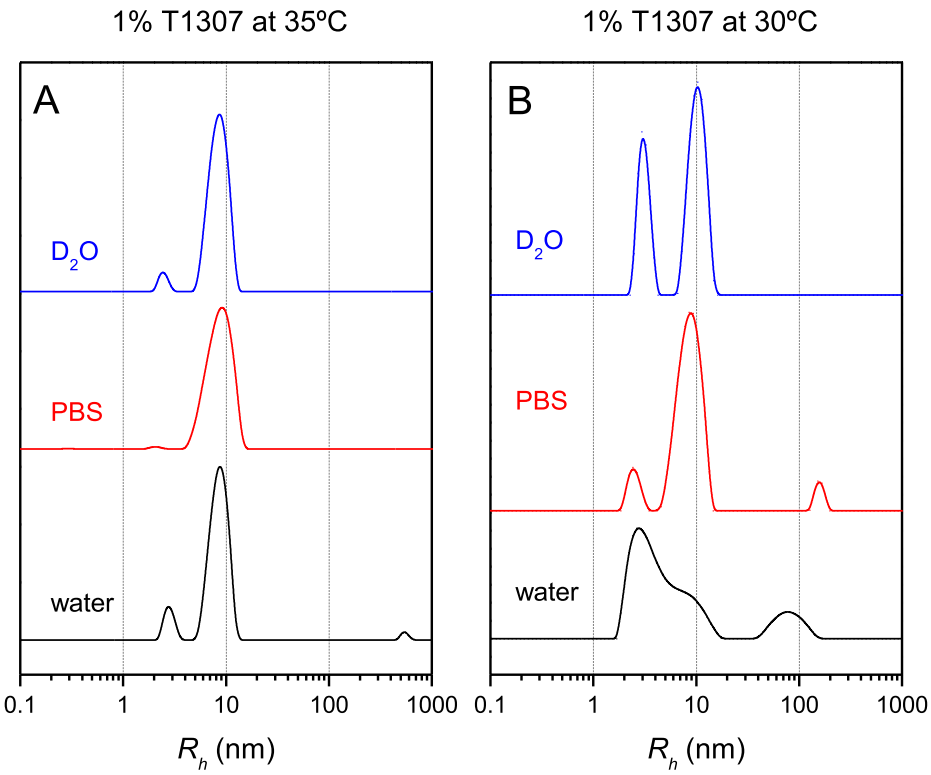

Fig. 2. DLS size distributions for 1% T1307 in water, PBS, and D_2O at 30 °C and 35 °C.

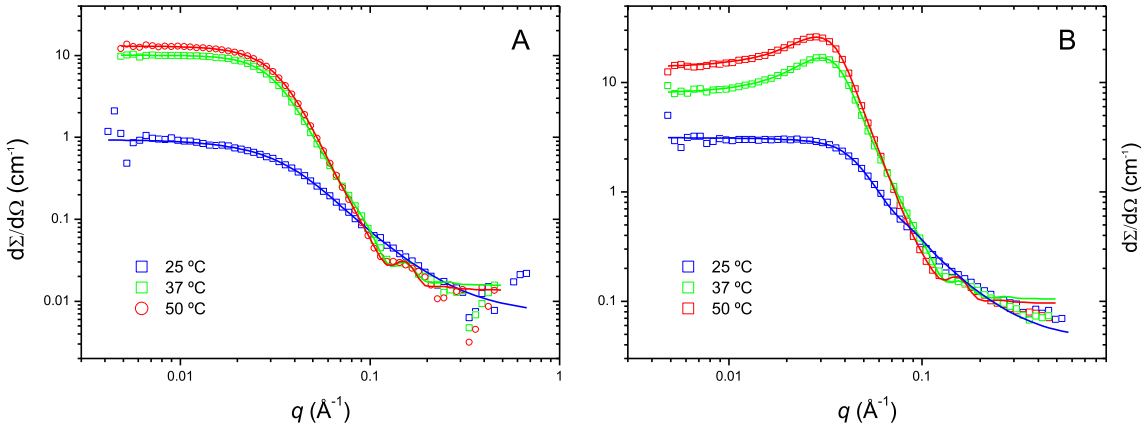

Fig. 3. SANS patterns of T1307 in deuterated PB as a function of the temperature at: (A) 1% T1307; (B) 5% T1307. Solid lines are the fits to a 4-star polymer (25 °C) and core–shell ellipsoids (37 °C, 50 °C).

respectively) [43]. At the buffered pH of the solution (7.4), the partial ionization of the linker group (Gonzalez-Lopez et al., 2008) [7] may contribute to this expansion, compared to the non-buffered medium. At higher concentration, the Gaussian model has to take into account the inter-polymer interactions, which have been modelled with a hard-sphere structure factor. At this concentration and 25 °C, the unimers R_g is 55 Å (Fig. 3b).

Micelles are fully formed at 37 and 50 °C, as evidenced from the change in the scattering patterns and the higher intensity (Fig. 3). Previous SANS studies on T1307 [43] and other poloxamines [8,49,50] described micelles as spheres with a "dry" core and a highly hydrated shell. This model can be acceptable at the pH of poloxamines in water (around 8) but it may not be adequate under conditions at which a considerable extent of unimers is protonated the charge distribution on the surfactant upon protonation may distort the ideal spherical shape of the aggregates. In addition, the assumption of a "dry" core may be an oversimplification under these conditions. Consequently, we have used a more realistic model to describe the aggregates at buffered pH, in which the core may incorporate solvent and the geometry is not constrained to a sphere, but micelles can elongate to adopt an ellipsoidal shape (see the SI for the description of the model and fit procedure). Likewise, we have considered that a fraction of the total EO can be present in the core. Table 1 shows the description of the parameters and their fitted values according to this theoretical model (fitted curves are represented as solid lines in Fig. 3).

Under the experimental conditions used, the micelles adopt the form of prolate ellipsoids (average axial ratio 1.5). The reduction in micellar size at 5% of the surfactant compared with 1% is in accordance with our DLS findings. The shell is highly hydrated, as

Table 1
Micellar parameters obtained from SANS data analysis for T1307 in phosphate buffer (pH 7.4), at different concentrations and temperatures. R_{eq} (equatorial radius of the core, Å); t_{eq} (thickness of shell at equator, Å); *x-core* (axial ratio of core); *x-shell* (ratio of thickness of shell at pole to that at equator); φ (particles volume fraction); ρ_s (shell scattering length density, $\times 10^6$ Å^2); ρ_c (core scattering length density, $\times 10^6$ Å^2); N_{agg} (aggregation number); $x_{D2O\ shell}$ (volume fraction of solvent in the shell); $y_{D2O\ core}$ (volume fraction of D_2O in the core); $y_{EO\ core}$ (volume fraction of EO in the core); $y_{PO\ core}$ (volume fraction of PO in the core); $y_{MF\ core}$ (volume fraction of MF in the core); $p_{EO\ shell}$ (proportion of EO in the shell).

	1%		5%	
	37 °C	**50 °C**	**37 °C**	**50 °C**
R_{eq}	34.8	36.2	32.2	35.3
t_{eq}	43.5	38.8	43.4	39.9
x-core	1.5	1.4	1.65	1.5
x-shell	1.9	2.1	1.18	1.48
φ	0.06	0.05	0.2	0.19
ρ_s	5.8	5.6	5.88	5.67
ρ_c	1.35	1.14	1.44	1.19
N_{agg}	20 (19)[†]	22 (20)	16 (21)	19 (23)
$x_{D2O\ shell}$	0.9	0.88	0.92	0.89
$y_{D2O\ core}$	0.16	0.13	0.17	0.13
$y_{EO\ core}$	0.17	0.16	0.29	0.23
$y_{PO\ core}$	0.67	0.72	0.54	0.61
$p_{EO\ shell}$	0.87	0.89	0.64	0.79

[†] Between parentheses: aggregation number calculated from the hard spheres volume fraction.

expected, but the core contains a substantial amount of solvent. Overall, about 83% of the volume of the micelle corresponds to solvent, of which just 1.3% is in the core. When increasing the temperature, solvent molecules are expelled from both the core and shell, producing "dryer" micelles. Several SANS and SAXS studies have shown significant amounts of water in the core of Pluronic micelles that decrease with the temperature [51,52]. The core also contains a significant amount of PEO that increases with the concentration of surfactant. Regarding the aggregation numbers, they are higher to those found at natural pH (13 at 40 °C and 19 at 50 °C, [43] tending to rise with the temperature and decrease with the surfactant concentration.

3.1.2. Micellization of MF in buffered medium

Given its amphiphilic character, MF self-aggregates into micelles. The values of the CMC found in the literature depend on the solvent and method used for its determination, and CMCs as low as 3 μM have been measured [53]. A systematic study on the aggregation of MF [54] in different media by probe fluorescence spectroscopy and surface tension has reported values that range from 60 μM in pure water to 35 μM in PBS (150 mM NaCl), which evidence non-negligible electrostatic effects on the micellization, in line with the zwitterionic nature of the drug. As in T1307, the CMC has been determined by using pyrene fluorescence emission (Fig. S3a), resulting in 60 μM in PBS (0.0024%). With respect to the temperature effect on the micelle sizes, they are nearly constant (ca. 3 nm) over the range studied in this work (Fig. S3b),

The micelle structure has been investigated by SANS at buffered pH = 7.4 (Fig. S4). The micellar model used assumes spherical core–shell micelles with a "dry core" and a hydrated shell, including a hard-spheres structure factor to account for the interactions. The increased scattering that can be observed at low q can be ascribed to the formation of large aggregates, also detected in DLS even after filtering the samples. The contribution of these nonspecific aggregates to the scattering has been taken into account by adding a power-law term to the function used to fit the data (leaving out the points at low q from the fits led in all cases to micellar sizes that were higher than those observed by DLS). The parameters found are collected in Table 2 (see the SI for the calculation of sld values and the mathematical model used).

There are no remarkable differences when comparing the fitted parameters with those of the drug in the non-buffered medium [29]. The micelle radius is only slightly higher in PB, although the apportioning between core radius and shell thickness is different. In buffered medium, the core radius is lower than the length of a fully extended chain of 16 carbons (22 Å, according to Tanford's formula, l = 1.55 + 1.265n_c, [55]). The fitted ρ_s suggests a less hydrated shell compared to water, although a certain extent of bound ions would also contribute to lowering its sld (the PB solution in our experiments contains 20 mmol/L of Na and 1.8 mmol/L of K, while MF is ca. 5 mmol). The incorporation of ions to the shell would also agree with the apparent extended shell thickness observed. However, a systematic study on the effect of the ionic strength covering a wider range of salt concentration would be necessary to confirm this point. Regarding the aggregation numbers, they increase approximately in a 10% in the buffered medium, in line with the small expansion of the micelle radius. Finally, the fitted exponent in the power law, m, is 2.45 (as obtained assuming it remains constant with the temperature). This value, intermediate between 2 and 3 mass fractal Porod exponents, indicates that the scattering at low q corresponds to a clustered network, although data at a lower q range should be necessary to confirm this point. In any case, the mass proportion of these large, unspecific aggregates must be very low, according to the DLS data (Fig. S3).

3.1.3. Mixed micelles T1307-MF: The diluted regime

The amphiphilic character of both T1307 and MF facilitates the formation of mixed micelles, whose structure varies with the proportion of both surfactants, as it will be shown below. Fig. 4 shows the DLS size distributions of a mixture 0.2% MF and 1% T1307 in PBS over a wide interval of temperatures. The distributions are monomodal in all cases and the hydrodynamic radii vary between 4.5 nm and 6.4 nm, i.e. intermediate between the sizes of T1307 (9 nm) and MF (3 nm) micelles. The presence of poloxamine unimers is not detected, indicating that they must be aggregated together with the drug below the critical micelle temperature (CMT) of the block copolymer.

Fig. S5c shows the 1D ^{1}H NMR spectrum of the mixture MF + T1307 in deuterated PB, at 37 °C (above the CMT), compared to the surfactants alone (see proton assignation in Fig. S5a-b). The most noticeable shifts indicative of intermolecular interactions can be detected in the hydrophobic tail (*a* and *f*) and the zwitterionic head (*d* and *e*) of MF. In the poloxamine, protons *2* of the PO, and protons *3* of both EO and PO shift downfield. At 25 °C, the 2D NOESY spectrum (Fig. 5a) reveals distinct cross-peaks between the PO protons of the poloxamine and those of the hydrophobic part of MF (*a*, *b*, *c*, and *f*), as an indication of a close contact between both hydrophobic moieties and confirm the simultaneous presence of both surfactants in the aggregates. Remarkably, a slight cross-

Table 2
Micellar parameters obtained from SANS data analysis for 0.2% of MF in phosphate buffer (pH 7.4) at different temperatures. R_c (core radius, Å), t (shell thickness, Å), φ (volume fraction), ρ_s (shell scattering length density, $\times 10^6$ Å^2), N_{agg} (aggregation number), x_{D2O} shell (volume fraction of solvent in the shell).

	25°C	**37 °C**	**50 °C**
R_c	19.3	17.8	18.6
t	14.1	15.1	14.1
φ	0.0043	0.005	0.0047
ρ_s	3.9	4.01	4.04
ρ_c	−0.37	−0.37	−0.37
N_{agg}	128 (106)	115 (87)	114(92)
$x_{D2O\ shell}$	0.52	0.54	0.55

peak is detected between the protons of the polar part of MF (*d*) and those of the PPO block but not with the PEO ones, as an indication that the MF head is preferentially located in the micellar core, rather than in the shell. Diffusion NMR experiments performed above and below the CMT corroborate the formation of mixed micelles (Table 3). Below the CMT, T1307 and MF in the mixture diffuse more slowly than the surfactants alone (unimers and micelles, respectively, at this temperature). At 37 °C, the DOSY maps in Fig. 5b show a single diffusion mode for the mixture, producing an intermediate *D* value between those of the poloxamine and the MF micelles at this temperature. These results are in line with the hydrodynamic radii obtained from DLS (included in Table 3, for comparison). On the other hand, the CMCs of the mixed aggregates are in between the values of the surfactants alone. For example, for a molar composition 5:1 of MF to T1307 at 37 °C in PBS, the mixed micelles form approximately at 0.035% in T1307 (<CMC of T1307) and 0.007% in MF (>CMC of MF), as shown in Fig. S6. Overall, the evidence provided by NMR, DLS and fluorescence confirmed the formation of mixed micelles above and below the CMT of the poloxamine, picturing the drug located in its entirety in the hydrophobic core of the aggregates, preferentially.

i) Structure of MF-rich mixed micelles.

The structure of the mixed micelles has been investigated by SANS. In what follows, we have considered two different scenarios: the case of MF-rich aggregates and the case of poloxamine-rich aggregates. Fig. 6a represents the SANS pattern of a 1% T1307 + 0.2% MF mixture as a function of the temperature. Under these conditions, the molar ratio MF/T1307 is 9:1 (MF-rich), hence

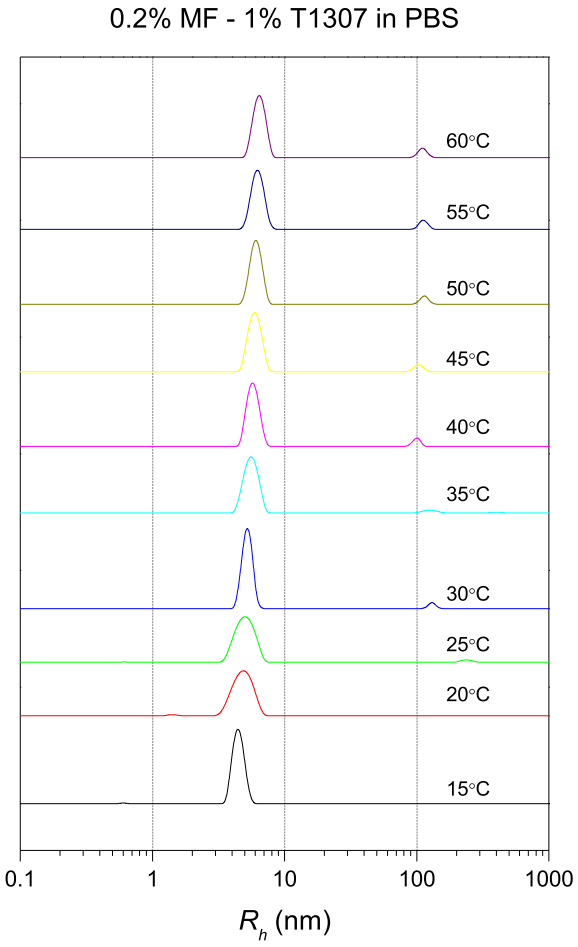

Fig. 4. DLS size distributions for of a mixture 0.2% MF and 1% T1307 in PBS as a function of the temperature.

we have modelled the system assuming core–shell ellipsoids with a dry core, as in MF micelles. Thus, the core does not contain EO from the poloxamine but only PO and, according to the NMR evidence, whole MF molecules (tail and head). Table 4 shows the fitted parameters obtained.

The low values of the ρ_c, similar to those of the MF micelles, support the assumption of the dry core, while the relatively high ρ_s indicates an extensive hydration of the shell. The total dimensions are intermediate between those of T1307 and MF micelles, as expected, with axial core ratio ($x = R_{polar}/R_{equatorial}$) slightly lower than for T1307. The aggregation number of poloxamine, N_T, can be deduced directly from the sld of the shell, which contains all the PEO blocks and a large number of solvent molecules

$$N_T = V_{shell}(1 - x_{D2O,shell})/V_{EO}$$

V_{shell} being the volume of the shell (calculated from the dimensions of the ellipsoid), V_{EO} the volume of the EO part of the poloxamine, and $x_{D2O,shell}$ the volume fraction of solvent in the shell. The number of drug molecules in the core, N_{MF}, can be obtained from the core dimensions, according to:

$$N_{MF} = (V_{core} - N_T V_{PO})/V_{MF}$$

Where V_{core} is the volume of the core, V_{PO} the volume of the PO part of T1307, and V_{MF} the volume of a MF molecule. In this model, there is no assumption of a fixed molar ratio, yet the calculated N_{MF}/N_T values are close to the stoichiometric ones at 37 °C and 50 °C. Above the CMT (37 °C and 50 °C), the poloxamine has a thermodynamic tendency to self-aggregate and the scenario is a mixed micelle in which all the poloxamine and the MF are forming the aggregates. The case of the mixtures at 25 °C is different since at this temperature the T1307 would be in the form of unimers. Fig. S7 shows a comparison between the SANS traces of T1307, MF and their mixture in a linear scale of intensity from Fig. 6 for better understanding. The fact that the curve for the mixture is not just the sum of the traces of the components alone indicates the formation of an "intermediate" structure between poloxamine unimers and MF micelles, in line with the DLS evidence and the measured diffusion coefficients by NMR at 25 °C. On the other hand, at this temperature, the ratio N_{MF}/N_T (Table 4) is lower than the stoichiometry, indicating an excess of free MF that, given the low CMC of the drug, must be in the form of micelles, its contribution to the total scattering being negligible.

ii) Structure of poloxamine-rich mixed micelles.

The amount of MF (0.2%) has been kept constant and increased the content in T1307 up to 3% and 5%. Fig. 6b represents the SANS traces for a composition 5% T1307:0.2% MF. The total scattering increases with the temperature, and the presence of the peak at around 0.03 $Å^{-1}$ indicates the inter micelle interactions that occur even at 25 °C (they do not appear for T1307 alone at this concentration). Considering the difference in size between both molecules, the situation would rather correspond to a T1307 micelle that includes MF molecules. Under these conditions (molar ratios MF/T1307 of 3 and 1.8, respectively), the assumption of a core that does not contain solvent or EO monomers is not reasonable. Hence, we have modified the theoretical model to fit the T1307 mixed micelles by incorporating into the equations the contribution of MF to the core volume and ρ_c. According to the previous results, we have imposed the condition that there is a complete mixing of the components in the micelles (the molar ratio $R = N_{MF}/N_T$ is fixed by the stoichiometry of the mixture). The set of independent relations between parameters (provided in the SI for the model proposed) lead to the following system of equations:

$$\rho_{core} - \rho_{D2O} = \{(\rho_{PO} - \rho_{D2O}) + R(\rho_{MF} - \rho_{D2O})\}\frac{v_{MF}}{v_{PO}}y_{PO} + (\rho_{PO} - \rho_{D2O})y_{EO}$$

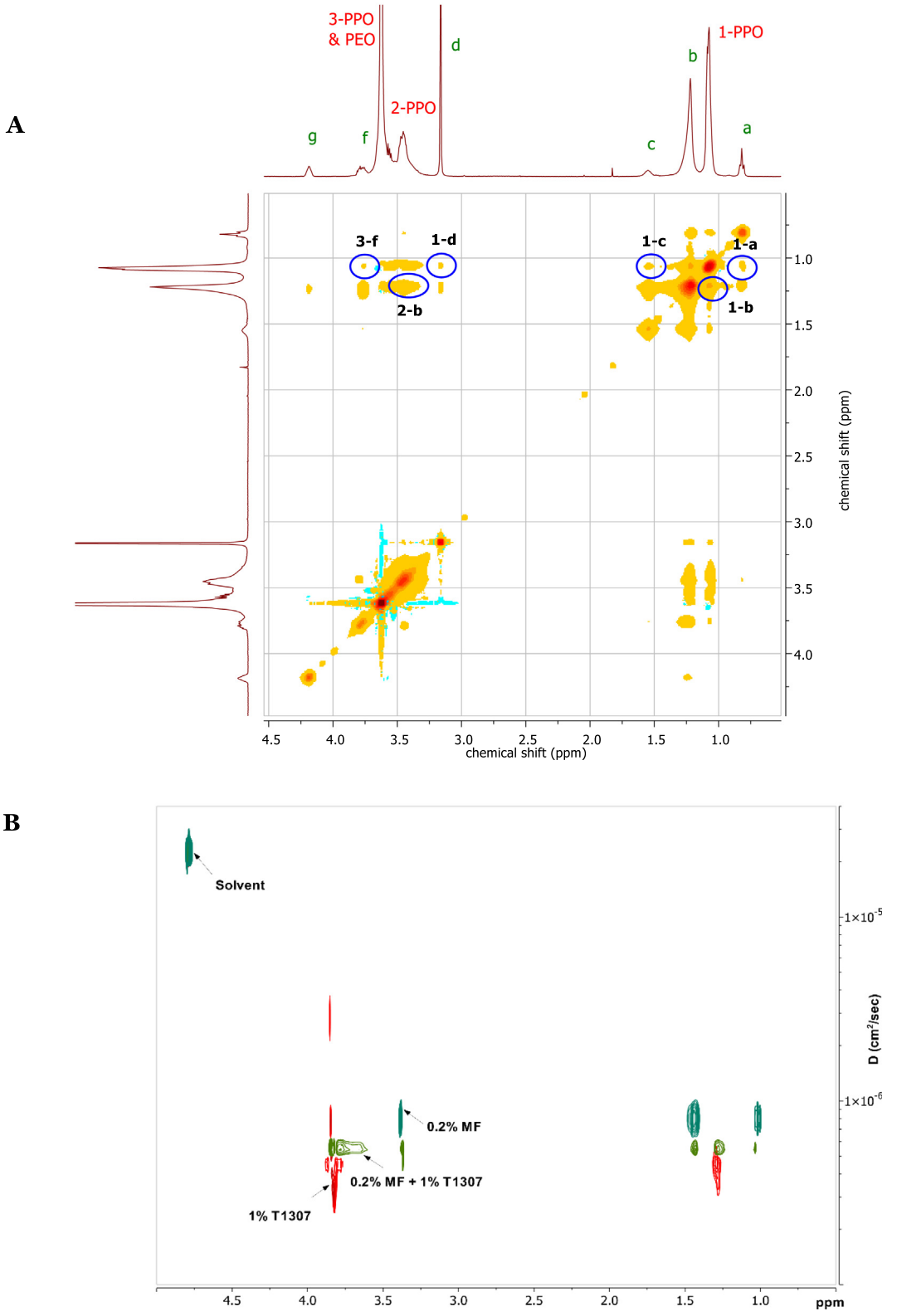

Fig. 5. (A) 2D-NOESY spectrum of 0.2% MF + 1% T1307 at 25°C. (B) DOSY maps of 1% T1307, 0.2% MF, and 1% T1307 + 0.2% MF at 37 °C.

$$V_{shell}\left(1 - x_{D2O,shell}\right) = V_{core}\frac{v_{EO}}{v_{PO}}y_{PO} - V_{core}y_{EO}$$

In which the unknowns are the volume fraction of EO and PO in the core, y_{EO} and y_{PO}, respectively. ρ_{core}, V_{core}, and V_{shell} are returned or deduced from the fits, while v_{EO}, v_{PO}, v_{MF} and the corresponding scattering length densities, as well as ρ_{D2O}, are introduced as constants at each temperature (see the SI for details on their calculation). The system has been solved for the different compositions and temperatures and the resulting fitted parameters have been collected in Table 4.

Table 3
Diffusion coefficients ($\times 10^7$ cm^2 s^{-1}) obtained from DOSY NMR for 1% T1307, 0.2 % MF and their mixture (25 °C and 37 °C, in deuterated PB). Between parentheses, the corresponding values obtained from DLS measurements.

	25°C	37 °C
1% T1307	5.23 (5.5)	3.15 (2.9)
0.2% MF	5.1 (5.8)	7.66 (7.9)
Mixture	3.78 (3.1)	5.36 (3.9)

In general, the values obtained from all the parameters reflect an intermediate situation between MF and poloxamine micelles. Thus, the shell is very hydrated, and the water content diminishes with the temperature, while the ρ_c is now higher than for the MF-rich mixture, reflecting the presence in the core of solvent and EO from the poloxamine. The mixed micelles are also larger as compared to the MF-rich case but smaller than in a 5% T1307 solution. The water content in the core, y_{D2O}, in the poloxamine-rich case is considerably lower (nearly zero at 3%), the proportion of EO in the core, y_{EO}, being only slightly lower than in the case of the poloxamine alone (see values in Tables 1 and 4). The aggregation numbers deduced from the model are also intermediate between those of MF and T1307 micelles.

In summary, MF and Tetronic combine at very different proportions and temperatures, even below the CMT of the poloxamine. This compatibility follows from the amphiphilic character of both components, with important consequences for the biological activity of the formulations, as shown below.

3.1.4. The concentrated regime: MF-loaded micellar gels

A potential application of the formulations MF-T1307 woul be its use in the form of gel for the delivery of MF through skin, which entails investigating the region of highly concentrated solutions of Tetronic. Fig. 7 represents the different phases of T1307 in water, PBS and D_2O. At 20% of T1307, the gel phase spans from 45 to 55 °C in water, while in PBS only a highly viscous solution is observed in this range (from 40 to 60 °C in D_2O). At higher surfactant concentrations, the gel region expands to a wider interval of temperatures and the onset of gelation diminishes, starting at 25 °C for 25% in PBS and 30 °C in D_2O, and from 35 °C in water. At 30% of the Tetronic, the gel forms from 22.5 °C to 70 °C in any of the solvents considered. In general, the proportion of MF in a formulation must be necessarily small, and no remarkable changes are expected in the gel properties. For example, at 24% T1307-1% MF in deuterated PB, the gel forms at 25 °C.

The structure of the physical gels in deuterated PB has been studied by SANS. Fig. 8a shows the scattering of a 25% T1307 solution at different temperatures. According to the phase diagram, the gel is fully formed at 37 and 50 °C and the scattering pattern reflects the paracrystalline packing of micelles in the sharp peaks at 0.048, 0.067 and 0.083Å^{-1}, which correspond to a BCC lattice (q/q_o = 1, $\sqrt{2}$, $\sqrt{3}$...), typical of these poloxamines [43,49,50]. Interestingly, although at 20 °C the solution is not a gel, the scattering reflects a high degree of micelle organization. In the model used to fit the data, the sld of the spheres was set to that of the core for a 5% solution at the temperature considered and the background taken as the limiting value at high q, leaving as floating parameters the scale (volume fraction of crystal in the sample volume), distance to nearest neighbor (dnn) and paracrystal distortion factor, d. The results are collected in Table 5.

The calculated sphere radii at 25% are smaller than those of the core size of T1307 micelles in the diluted regime, assuming spherical shape. According to the calculated dimensions of the paracrystal cell, a, the shell would expand up to a total sphere radius of 80 Å (R_{mic} = $\sqrt{3}/4a$), if we consider a compact packing in which the spheres are in contact along the diagonal of the BCC unit. This value is slightly lower than the size of the micelles in the dilute regime (Table 1), which implies certain overlap between shells of adjacent micelles, as it occurs with other hydrophilic members of the Tetronic® family [38]. The lattice parameter is virtually constant with the temperature and, similarly to the diluted regime, the micelle radius increases moderately. The volume fraction of crystal is lowest at 20 °C, indicating that the gel is not fully formed at this temperature.

This same model has been applied to mixtures containing 24.8% T1307-0.2% MF and 24% T1307-1% MF. Given the small proportion of the drug (molar ratio MF/T1307 of 0.4 and 1.8, respectively), noticeable changes in the gel structure are not expected. Moreover, the diffraction peaks are clearly shifted with respect to the 25% of poloxamine (Fig. 8b), as an indication that the dimensions of the paracrystalline lattice are smaller (Table 5). The trend in the micelles size is in line with the proportion of MF, being in all cases smaller than for the poloxamine alone at 25% (the higher the proportion of drug, the smaller the size and the lattice spacing, the temperature tending to increase both).

In conclusion, the combinations MF-T1307 at high concentration of Tetronic form physical gels by packing of the mixed micelles, in which the paracrystalline structure of the poloxamine is preserved. The effect of the presence of MF is a reduction in the onset of gelation and, at a mesoscopic level, the smaller sizes of the packed micelles, depending on the proportion of the drug.

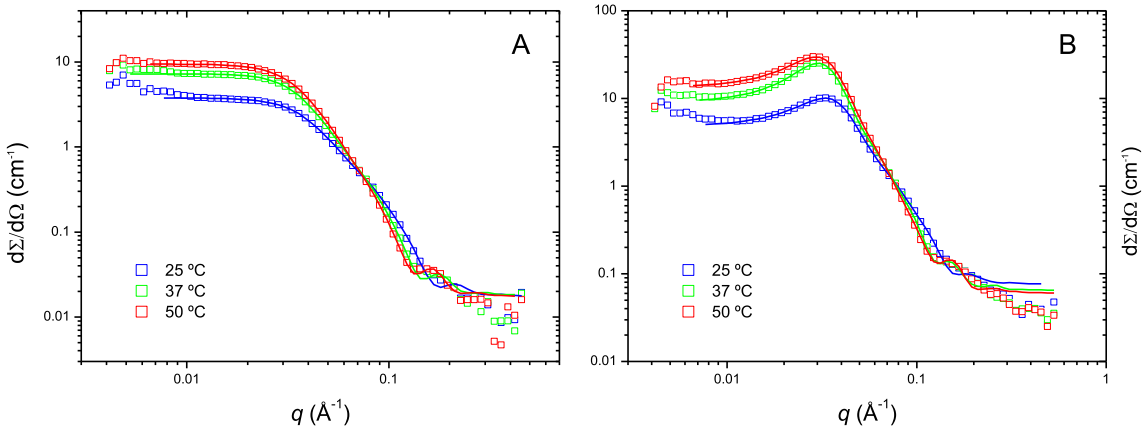

Fig. 6. SANS patterns of mixtures (A) 1% T1307 – 0.2% MF; (B) 5% T1307 – 0.2% MF in deuterated PB as a function of the temperature. Solid lines are the fits to core–shell ellipsoids.

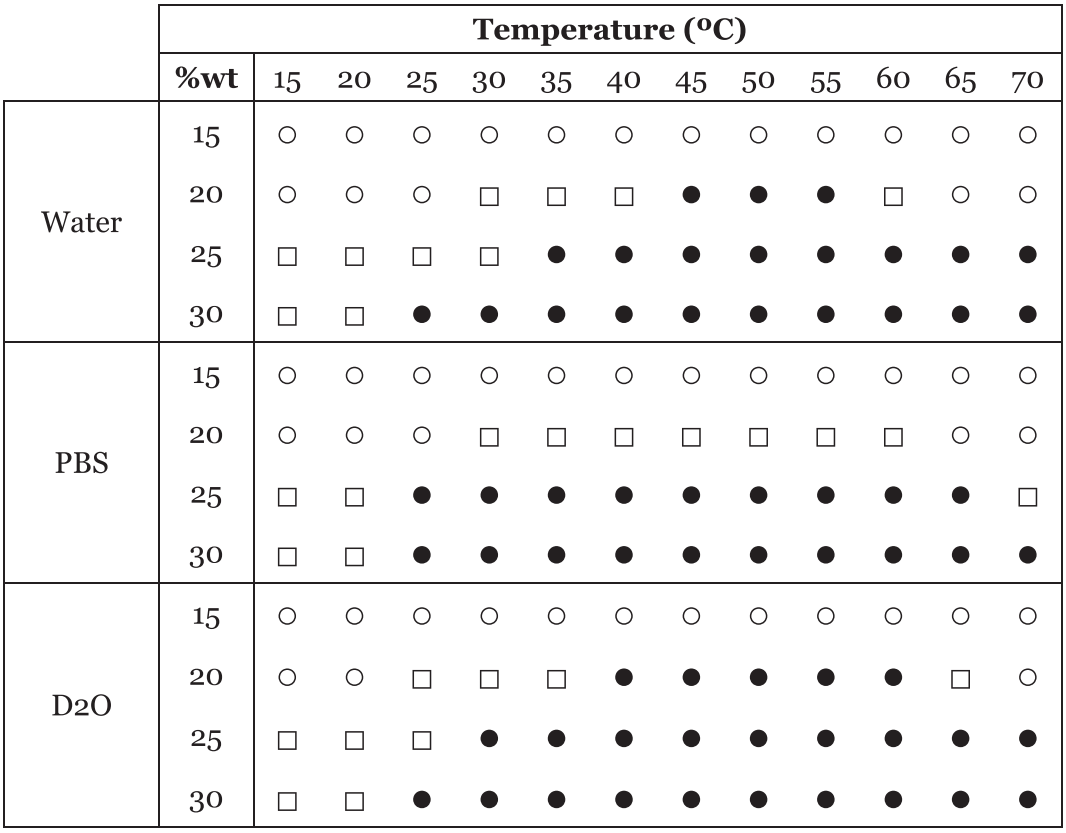

Fig. 7. T1307 phase behaviour in different solvents. ○ solution; □ viscous solution; ● gel.

Table 4
Micellar parameters obtained from SANS data analysis for mixed micelles of T1307 + 0.2% MF, at different poloxamine concentrations and temperatures. R_{eq} (equatorial radius of the core, Å); t_{eq} (thickness of shell at equator, Å); *x-core* (axial ratio of core); *x-shell* (ratio of thickness of shell at pole to that at equator); φ (particles volume fraction); ρ_s (shell scattering length density, $\times 10^6$ Å^2); ρ_c (core scattering length density, $\times 10^6$ Å^2); N_{agg} (aggregation number); $x_{D2O\ shell}$ (volume fraction of solvent in the shell); $y_{D2O\ core}$ (volume fraction of D_2O in the core); $y_{EO\ core}$ (volume fraction of EO in the core); $y_{PO\ core}$ (volume fraction of PO in the core); $y_{MF\ core}$ (volume fraction of MF in the core); $p_{EO\ shell}$ (proportion of EO in the shell).

	T1307 – 0.2% MF								
	1%			3%			5%		
	25°C	37°C	50°C	25°C	37°C	50°C	25°C	37°C	50°C
R_{eq}	24.4	29.7	32.5	25.3	33.4	34.4	27.1	34.2	35
t_{eq}	32	36.5	38.5	33.7	44	40.5	39.5	45.9	41
x-core	1.42	1.39	1.39	1.5	1.47	1.4	1.6	1.5	1.43
x-shell	2.6	2.2	1.9	2.47	1.56	1.7	1.53	1.33	1.61
φ	0.057	0.063	0.055	0.13	0.16	0.14	0.2	0.24	0.22
ρ_s	5.92	5.83	5.76	5.89	5.85	5.7	5.97	5.85	5.68
ρ_c	−0.704	−0.0156	−0.179	0.24	0.76	0.515	0.65	0.95	0.66
N_{T1307}	7	11	12	8	16	18	9	17	19
N_{MF}	38	83	127	25	46	52	16	30	33
$x_{D2O\ shell}$	0.92	0.91	0.9	0.92	0.91	0.89	0.93	0.91	0.89
$y_{D2O\ core}$	–	–	–	0	0.07	0.03	0.04	0.09	0.05
$y_{EO\ core}$	–	–	–	0.1	0.18	0.17	0.28	0.24	0.21
$y_{PO\ core}$	–	–	–	0.74	0.61	0.65	0.6	0.59	0.65
$y_{MF\ core}$	–	–	–	0.17	0.14	0.15	0.08	0.08	0.09
$p_{EO\ shell}$	–	–	–	0.93	0.85	0.87	0.77	0.8	0.84

3.2. Biological evaluation of the formulations

(i) Cytotoxicity assays

After the structural characterization of the aggregates, their cytotoxicity was evaluated in murine macrophages, the primary host cells infected by *Leishmania* parasites. It is known that T1307 and some other poloxamines have shown cytotoxic effects at specific concentrations (1–5%), when tested against fibroblast and epithelial cell lines [49,56]. Therefore, the toxicity on macrophages was tested up to 5% T1307 (Tables 6 and S1). Our results showed that, at concentrations higher than 1.5%, T1307 exhibited toxicity (cell viability < 80 %, towards macrophages) (Table S1). Accordingly, 1% T1307 was the maximal concentration used in the further biological studies. On the other hand, the cytotoxicity of MF was studied in the range of 0–25 μM. The half-maximal cytotoxic concentration (CC_{50}) was 12.99 μM (with P95 confidence limits between 12.69 and 13.3 μM). This result supported previous publications describing 38–60% cell death in macrophages treated

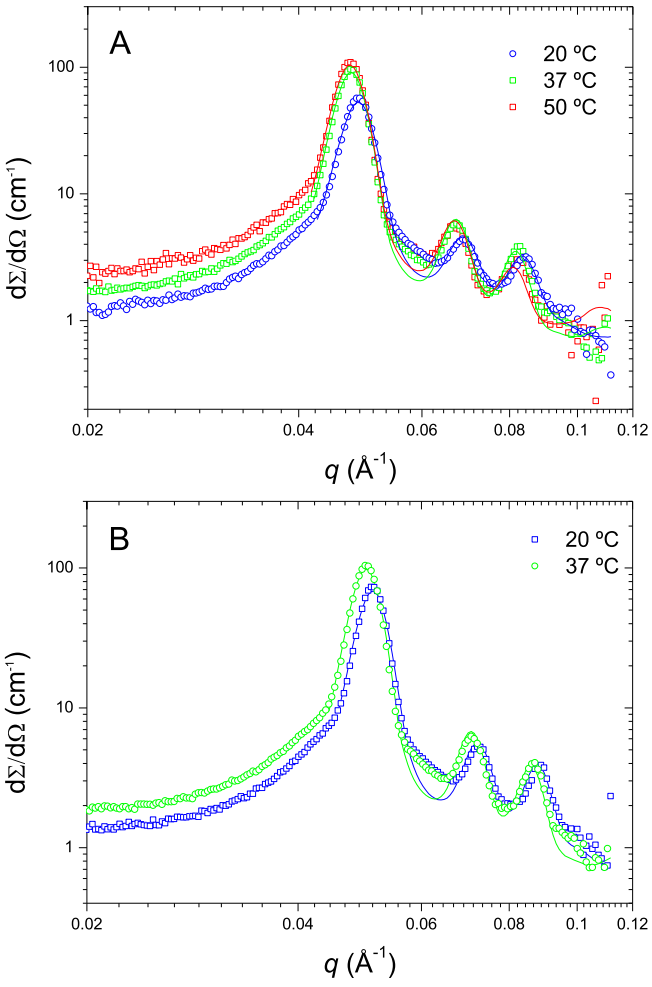

Fig. 8. SANS patterns of (A) a 25% solution of T1307; (B) a mixture 24% T1307 – 1% MF, both in deuterated PB. Solid lines are the fits to a BCC paracrystal model.

with 9–18 μM MF [57]. Table 6 displays the percentage of macrophage viability (83.4%) after 48 h of treatment with 12 μM MF, while the combinations MF-T1307 did not present toxicity (100% cell viability). Altogether, these data reveal that the encapsulation of 12 μM MF within T1307 micelles completely prevents the toxic effect of 12 μM free MF (Table 6).

ii) Activity against *Leishmania major* parasites.

Since 1% T1307 and 1% T1307- 12 μM MF formulations did not display toxicity towards macrophages, their biological effects on intracellular amastigotes were assessed. *L. major* infected macrophages were treated for 48 h with T1307-MF mixtures at two concentrations (0.0625 and 1 %) of T1307 and at 12 μM MF. As shown

Table 6
Percentage of cell viability of murine macrophages at 48 h post-treatment with T1307 (0–1%), MF (0–12 μM) and their combinations.

		T1307		
		0%	**0.063%**	**1%**
MF	**0 μM**	100	100	100
	12 μM	83.4 ± 1.46	100	100

in Fig. 9a, the T1307-MF combinations significantly reduced the percentage of amastigotes per macrophage. In comparison to untreated cells (100% infection), there were dramatic reductions when treated with T1307-MF formulations: 55.60% with 0.0625% T1307-12 μM MF (*, $p < 0.05$) and 26.26% with 1% T1307-12 μM MF (**, $p < 0.01$). Moreover, 1% T1307 *per se* exhibited a leishmanicidal activity and significantly reduced the amastigote burden by approximately 50% (44.38 % vs 100.00 %: **, $p < 0.01$). In contrast, *L. major* was less sensitive to MF alone at 12 μM (94.55 ± 7.71 % of amastigotes/macrophage) supporting the data from Escobar *et al.* (2002) [58]. These authors reported an IC_{50} > 30 μM for MF on *L. major* amastigotes [58]. On the other hand, we found that MF was also active on promastigotes (IC_{50} = 6.21–12.35 μM), in accordance with values (IC_{50} = 4.80 – 13.10 μM) published by these researchers in *L. major* [58]. On both forms of the parasite, the combination 1% T1307-12 μM MF was the most potent formulation, showing a leishmanicidal activity > 95% on promastigotes and > 75% on amastigotes (Fig. 9). Interestingly, this formulation significantly enhanced the activity of MF by 3.6-fold and 16-fold on *L. major* intracellular and extracellular forms, respectively.

Tetronic surfactants had been highly active against cancer cell lines at concentrations between 0.01% and 1% [59,60]. In addition, triblock copolymers were also effective as nanocarriers for the treatment of some infectious diseases, including leishmaniasis [29,61]. The use of these systems improved the antimicrobial effects and lowered the cytotoxicity of the drugs supporting the results obtained in the present study. The direct biological effect of PEO-PPO-PEO blocks previously described [62], as well as the interaction of these polymers with the membrane lipid bilayers [63], might shed some light on the antileishmanial activity of T1307 observed in this work (Fig. 9). However, more research would be neccesary to fully understand the precise mechanisms of action.

4. Conclusions

Here we propose the use of block copolymer Tetronic 1307 (T1307) as a nanocarrier of miltefosine (MF), an amphiphilic alkylphospholipid highly active against leishmaniasis. The starting hypothesis is that, given the amphiphilic nature of MF, both surfactants will combine to form mixed micelles and gels that allow reducing the cytotoxicity of the drug by lowering its dose and

Table 5
Parameters obtained from SANS data analysis to a BCC lattice of T1307 and mixtures with MF in deuterated phosphate buffer. R_c (radius of the core, Å); *dnn* (distance to nearest neighbour, Å); R_m (micelle radius, calculated from *dnn*); φ (volume fraction of paracrystal in sample volume); *d* (paracrystal distortion factor); ρ_c (core scattering length density, $\times 10^6$ Å^2).

Parameters	**25% T1307**			**24.8% T1307 - 0.2% MF**			**24% T1307 - 1% MF**	
	20°C	**37°C**	**50°C**	**20°C**	**37°C**	**50°C**	**20°C**	**37°C**
φ	0.389	0.483	0.399	0.447	0.570	0.497	0.401	0.495
dnn	158	162	162	156	156	157	150	154
d	0.064	0.049	0.052	0.052	0.047	0.050	0.057	0.050
R_c	41	46	48	42	44	47	40	43
R_m	79	81	81	78	78	79	75	77
ρ_c	1.4	1.4	1.1	0.6	0.9	0.7	0.6	0.9

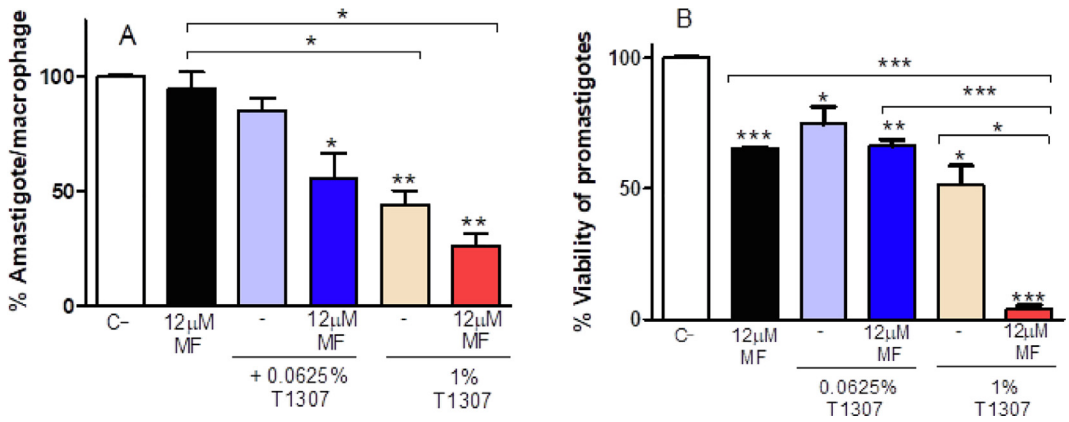

Fig. 9. Effect of MF, T1307, and T1307-MF on *L. major* amastigotes (A) and promastigotes (B). Treatments were performed for 48 h at different concentrations: MF (12 μM), T1307 (0.0625% and 1%), and T1307-MF (0.0625%-12 μM, 1% −12 μM). Bars represent the percentage of amastigotes/infected macrophages (A) and the percentage of cell viability of promastigotes (B) with respect to the control (untreated cells, C-). P-Values < 0.05 (*), <0.01 (**), <0.001 (***) were considered significant.

improving its cell internalization. With this aim, we have undertaken a full structural characterization of the surfactants on their own and their combinations in buffered medium (pH = 7.4) and as a function of the temperature and concentration, as well as the biological evaluation of the formulations.

Regarding the poloxamine, its aggregation is favoured in buffered medium with respect to water or D_2O, as evidenced by DLS and fluorescence spectroscopy. SANS experiments are consistent with the formation of ellipsoidal micelles with a highly hydrated shell (90%) in which the EO apportions between the shell and core, and there is a considerable amount of water in the core, rather than the spherical and "dry" micelles reported in the literature in non-buffered medium. Micelles with higher aggregation number and less content in water form when increasing the temperature, while the concentration tends to reduce the aggregates size. By contrast, MF self-aggregates into "classical" spherical micelles, having a "dry core", formed by the hydrocarbon chain of the drug, and the shell formed by the zwitterion head and water. There is a slight reduction in the aggregation number as the temperature increases and no remarkable effects due to the buffered medium.

When combining both surfactants, DLS, diffusion NMR and probe fluorescence spectroscopy support the formation of mixed micelles. The 2D NMR data prove that the whole drug, and not just the hydrocarbon tail, is in close contact with the PPO moieties (micelle core) but not with the PEO. Two scenarios arise depending on the proportion of both surfactants (MF-rich micelles versus T1307-rich micelles). These different situations have been considered into the analysis of the SANS data according to a model that assumes ellipsoidal aggregates than lodge the MF, water and EO in their core. In MF-rich micelles below the CMT of the poloxamine, the low values of ρ_c and the failure of the model to account for the EO and water in the core, evidence the formation of dry-core aggregates, similar to the MF micelles. When the temperature increases, the core expands and incorporates water and some EO from the poloxamine. In a T1307-rich scenario, the higher ρ_c values reflect the presence of water and EO, as in T1307 micelles. Mixed micelles also form at 25 °C, below the CMT of the poloxamine, but the tendency to incorporate MF increases with the temperature. Overall, the MF and T1307 combine at every proportion and temperature to form mixed micelles, their structure reflecting their different amounts present. At high concentrations of T1307 (25%), the gelation of the system occurs, with a BCC paracrystal packing of micelles. The addition of MF produces a shift in the diffraction peaks compared to the T1307 alone that reflect a smaller size of the paracrystal cell, the effect being more marked the higher the proportion of drug is.

Biological studies on *L. major* promastigotes and amastigotes, combined with cytotoxicity studies in the host macrophages, lead to identify a potent formulation, composed of 1%T1307-12 μM MF. The reformulated drug is more active and less toxic, which could be related to a better internalization and targeting produced by the poloxamine. Besides acting as a carrier, T1307 micelles *per se* are also active against both forms of the parasites, reducing the parasitic intracellular load and the promastigotes survival by almost 50%, at 1% of poloxamine concentration.

In conclusion, the results herein support the use of the hydrophilic Tetronic 1307 as a carrier of MF for the treatment of leishmaniasis. Drug loaded polymeric micelles could be administered topically in different forms, as a viscous liquid that evolves into gel in contact with the skin or as a cream [16,41], or as droplets of a liquid solution [64]. Such formulations would prevent the gastrointestinal side effects related to the oral intake of the drug. The of MF with poloxamines in the form of mixed micelles seems a promising strategy to treat both human and animal leishmaniasis, their joint use with other antiparasitic agents that can be incorporated to the aggregates.

CRediT authorship contribution statement

Zeinab Dirany: Methodology, Investigation, Writing – original draft, Writing – review & editing, Visualization. **Rima El-Dirany:** Investigation. **Gregory N. Smith:** Investigation, Data curation, Writing – original draft, Writing – review & editing, Resources. **Paul Nguewa:** Supervision, Conceptualization, Methodology, Investigation, Writing – original draft, Writing – review & editing, Project administration, Funding acquisition, Resources. **Gustavo González-Gaitano:** Supervision, Conceptualization, Investigation, Writing – original draft, Writing – review & editing, Visualization, Project administration, Funding acquisition, Resources.

Data availability

Data will be made available on request.

Declaration of Competing Interest

The authors declare that they have no known competing financial interests or personal relationships that could have appeared to influence the work reported in this paper.

Acknowledgments

The authors gratefully acknowledge the financial support provided by "Ministerio de Ciencia e Innovación" from Spain (Project PID2020-112713RB-C21), *Fundación La Caixa* (LCF/PR/PR13/51080005), *Fundación Roviralta* and Ubesol and COST actions CA18217, CA18218, CA21105 and CA21111. Z. D. acknowledges the Asociación de Amigos (ADA) de la Universidad de Navarra for her doctoral grant. We acknowledge ISIS Neutron and Muon Source for beamtime on the LARMOR instrument. Data is available at https://doi.org/10.5286/ISIS.E.RB2210097. Prof. Carlos Aydillo is acknowledged by his help with the NMR experiments. We thank Celia Fernández-Rubio (PhD), Aroia Burguete (MSc) and Mikel Domeño for their technical support. Finally, this work benefited from the use of *SasView* 5.0.5 software, originally developed under NSF Award DMR-0520547. *SasView* also contains code developed with funding from the EU Horizon 2020 programme under the SINE2020 project Grant No 654000. For the purpose of open access, the author has applied a Creative Commons Attribution (CC BY) license to any Author Accepted Manuscript version arising.

Appendix A. Supplementary material

Supplementary data to this article can be found online at https://doi.org/10.1016/j.molliq.2023.121654.

References

[1] J. Puig-Rigall, M.J. Blanco-Prieto, A. Radulescu, C.A. Dreiss, G. González-Gaitano, Morphology, gelation and cytotoxicity evaluation of D-α-Tocopheryl polyethylene glycol succinate (TPGS) – Tetronic mixed micelles, J. Colloid Interface Sci 582 (2021) 353–363, https://doi.org/10.1016/j.jcis.2020.08.004.

[2] M. Ghezzi, S. Pescina, C. Padula, P. Santi, E. Del Favero, L. Cantù, S. Nicoli, Polymeric micelles in drug delivery: An insight of the techniques for their characterization and assessment in biorelevant conditions, J. Control. Release 332 (2021) 312–336.

[3] A. Figueiras *et al.*, "New Advances in Biomedical Application of Polymeric Micelles," *Pharmaceutics*, vol. 14, no. 8. MDPI, Aug. 01, 2022. doi: 10.3390/pharmaceutics14081700.

[4] S. Kotta, H. M. Aldawsari, S. M. Badr-Eldin, A. B. Nair, and K. YT, "Progress in Polymeric Micelles for Drug Delivery Applications," *Pharmaceutics*, vol. 14, no. 8. MDPI, Aug. 01, 2022. doi: 10.3390/pharmaceutics14081636.

[5] S. Perumal, R. Atchudan, and W. Lee, "A Review of Polymeric Micelles and Their Applications," *Polymers*, vol. 14, no. 12. MDPI, Jun. 01, 2022. doi: 10.3390/polym14122510.

[6] S.K. Hari, A. Gauba, N. Shrivastava, R.M. Tripathi, S.K. Jain, A.K. Pandey, Polymeric micelles and cancer therapy: an ingenious multimodal tumor-targeted drug delivery system, *Drug Deliv. Transl. Res.*. Springer 13 (1) (2023) 135–163.

[7] J. Gonzalez-Lopez, C. Alvarez-Lorenzo, P. Taboada, A. Sosnik, I. Sandez-Macho, A. Concheiro, Self-associative behavior and drug-solubilizing ability of poloxamine (tetronic) block copolymers, Langmuir 24 (19) (Oct. 2008) 10688–10697, https://doi.org/10.1021/la8016563.

[8] G. González-Gaitano, C. Müller, A. Radulescu, C.A. Dreiss, Modulating the self-assembly of amphiphilic X-shaped block copolymers with cyclodextrins: Structure and mechanisms, Langmuir 31 (14) (Apr. 2015) 4096–4105, https://doi.org/10.1021/acs.langmuir.5b00334.

[9] J. Puig-Rigall, R. Serra-Gómez, N. Guembe-Michel, I. Grillo, C.A. Dreiss, G. González-Gaitano, Threading Different Rings on X-Shaped Block Copolymers: Hybrid Pseudopolyrotaxanes of Cyclodextrins and Tetronics, Macromolecules 53 (8) (2020) 3166–3174.

[10] E. Larrañeta, J.R. Isasi, Non-covalent hydrogels of cyclodextrins and poloxamines for the controlled release of proteins, Carbohydr Polym 102 (1) (2014) pp, https://doi.org/10.1016/j.carbpol.2013.11.002.

[11] M. Almeida, M. Magalhães, F. Veiga, A. Figueiras, Poloxamers, poloxamines and polymeric micelles: Definition, structure and therapeutic applications in cancer, J Polym Res 25 (1) (2018).

[12] J.S. Park, S. Lee, D.H. Oh, P.L. Thi, K.D. Park, In situ Forming Hydrogel Crosslinked with Tetronic Micelle for Controlled Delivery of Hydrophobic Anticancer Drug, Macromol Res 30 (11) (2022) 811–819.

[13] S.A. Pillai, U. Sheth, A. Bahadur, V.K. Aswal, P. Bahadur, Salt induced micellar growth in aqueous solutions of a star block copolymer Tetronic® 1304: Investigating the role in solubilizing, release and cytotoxicity of model drugs, J Mol Liq 224 (Dec. 2016) 303–310, https://doi.org/10.1016/j.molliq.2016.09.091.

[14] M. Rodríguez-Évora, R. Reyes, C. Alvarez-Lorenzo, A. Concheiro, A. Delgado, C. Évora, Bone regeneration induced by an in situ gel-forming poloxamine, bone morphogenetic protein-2 system, J Biomed Nanotechnol 10 (6) (2014) pp, https://doi.org/10.1166/jbn.2014.1801.

[15] E. Larrañeta, J.R. Isasi, Phase behavior of reverse poloxamers and poloxamines in water, Langmuir 29 (4) (2013) pp, https://doi.org/10.1021/la304245p.

[16] R. El-Dirany, C. Fernández-Rubio, J. Peña-Guerrero, E. Moreno, E. Larrea, S. Espuelas, F. Abdel-Sater, K. Brandenburg, G. Martínez-de-Tejada, P. Nguewa, Repurposing the Antibacterial Agents Peptide 19–4LF and Peptide 19–2.5 for Treatment of Cutaneous Leishmaniasis, Pharmaceutics 14 (11) (Nov. 2022) 2528.

[17] T.P.C. Dorlo, M. Balasegaram, J.H. Beijnen, P. J. de vries,, Miltefosine: A review of its pharmacology and therapeutic efficacy in the treatment of leishmaniasis, J. Antimicrob. Chemother. 67 (11) (Nov. 2012) 2576–2597, https://doi.org/10.1093/jac/dks275.

[18] B. Monge-Maillo, R. López-Vélez, and L. D. Saravolatz, "Miltefosine for visceral and cutaneous leishmaniasis: Drug characteristics and evidence-based treatment recommendations," *Clinical Infectious Diseases*, vol. 60, no. 9. Oxford University Press, pp. 1398–1404, May 01, 2015. doi: 10.1093/cid/civ004.

[19] S.R.B. Uliana, C.T. Trinconi, A.C. Coelho, Chemotherapy of leishmaniasis: present challenges, Parasitology 145 (4) (2018) 464–480.

[20] S. Rijal *et al.*, "Increasing Failure of Miltefosine in the Treatment of Kala-azar in Nepal and the Potential Role of Parasite Drug Resistance, Reinfection, or Noncompliance," *Clinical Infectious Diseases*, vol. 56, no. 11, pp. 1530–1538, Jun. 2013, doi: 10.1093/cid/cit102.

[21] S. Sundar, A. Singh, M. Rai, V.K. Prajapati, A.K. Singh, B. Ostyn, M. Boelaert, J.-C. Dujardin, J. Chakravarty, Efficacy of Miltefosine in the Treatment of Visceral Leishmaniasis in India After a Decade of Use, Clin. Infect. Dis. 55 (4) (2012) 543–550.

[22] S. Srivastava, J. Mishra, A.K. Gupta, A. Singh, P. Shankar, S. Singh, Laboratory confirmed miltefosine resistant cases of visceral leishmaniasis from India, Parasit Vectors 10 (1) (Jan. 2017) 1–11, https://doi.org/10.1186/s13071-017-1969-z.

[23] J. Peña-Guerrero, J. Puig-Rigall, G. González-Gaitano, P. Nguewa, Chapter 13 - Improving the miltefosine efficacy against leishmaniasis by using different nanoassemblies made from surfactants or amphiphilic antimony (V) complex, in: F.R. Formiga, . Inamuddin, and P. Severino, (Eds.), Applications of Nanobiotechnology for Neglected Tropical Diseases, Academic Press, 2021, pp. 253–290, https://doi.org/10.1016/B978-0-12-821100-7.00013-3.

[24] J.K. Valenzuela-Oses, M.C. García, V.A. Feitosa, J.A. Pachioni-Vasconcelos, S.M. Gomes-Filho, F.R. Lourenço, N.N.P. Cerize, D.S. Bassères, C.O. Rangel-Yagui, Development and characterization of miltefosine-loaded polymeric micelles for cancer treatment, Mater. Sci. Eng. C 81 (2017) 327–333.

[25] M. Cagel, F.C. Tesan, E. Bernabeu, M.J. Salgueiro, M.B. Zubillaga, M.A. Moretton, D.A. Chiappetta, Polymeric mixed micelles as nanomedicines: Achievements and perspectives, Eur. J. Pharm. Biopharm. 113 (2017) 211–228.

[26] M. Algarabel, C. Fernández-Rubio, K. Musilova, J. Peña-Guerrero, A. Vacas, E. Larrea, P.A. Nguewa, In leishmania major, the homolog of the oncogene pes1 may play a critical role in parasite infectivity, Int J Mol Sci 22 (22) (Nov. 2021) 12592.

[27] J. Peña-Guerrero, C. Fernández-Rubio, A. Burguete-Mikeo, R. El-Dirany, A.T. García-Sosa, P. Nguewa, Discovery and validation of lmj_04_brct domain, a novel therapeutic target: Identification of candidate drugs for leishmaniasis, Int J Mol Sci 22 (19) (Oct. 2021), https://doi.org/10.3390/ijms221910493.

[28] A. Vacas, C. Fernández-Rubio, E. Larrea, J. Peña-Guerrero, P.A. Nguewa, LmjF.22.0810 from leishmania major modulates the TH2-type immune response and is involved in leishmaniasis outcome, Biomedicines 8 (11) (Nov. 2020) 1–17, https://doi.org/10.3390/biomedicines8110452.

[29] J. Puig-Rigall, C. Fernández-Rubio, J. González-Benito, J.E. Houston, A. Radulescu, P. Nguewa, G. González-Gaitano, Structural characterization by scattering and spectroscopic methods and biological evaluation of polymeric micelles of poloxamines and TPGS as nanocarriers for miltefosine delivery, Int J Pharm 578 (2020) 119057.

[30] Vacas, Fernández-Rubio, Algarabel, Peña-Guerrero, Larrea, Rocha Formiga, García-Sosa, Nguewa, The novel serine/threonine protein kinase lmjf.22.0810 from Leishmania major may be involved in the resistance to drugs such as paromomycin, Biomolecules 9 (11) (Nov. 2019) 723.

[31] C. Fernández-Rubio, E. Larrea, J. Peña Guerrero, E. Sesma Herrero, I. Gamboa, C. Berrio, D. Plano, S. Amin, A.K. Sharma, P.A. Nguewa, Leishmanicidal Activity of Isoselenocyanate Derivatives, Antimicrob Agents Chemother 63 (2) (2019).

[32] C. Fernández-Rubio, D. Campbell, A. Vacas, E. Ibañez, E. Moreno, S. Espuelas, A. Calvo, J.A. Palop, D. Plano, C. Sanmartin, P.A. Nguewa, Leishmanicidal activities of novel methylseleno-imidocarbamates, Antimicrob Agents Chemother 59 (9) (2015) 5705–5713.

[33] C.H. Cho, J. Urquidi, S. Singh, G.W. Robinson, Thermal offset viscosities of liquid H2O, D2O, and T2O, J. Phys. Chem. B 103 (11) (Mar. 1999) 1991–1994, https://doi.org/10.1021/jp9842953.

[34] H. Odhner, D.T. Jacobs, Refractive index of liquid D2O for visible wavelengths, J Chem Eng Data 57 (1) (Jan. 2012) 166–168, https://doi.org/10.1021/je200969r.

[35] G. González-Gaitano, A. Crespo, A. Compostizo, G. Tardajos, Study at a Molecular Level of the Transfer Process of a Cationic Surfactant from Water to β-Cyclodextrin, J. Phys. Chem. B 101 (22) (1997) 4413–4421.

[36] G. Gonzalez Gaitano et al., "Drug delivery systems based on micelles and gels of poloxamines and miltefosine-cyclodextrin complexes for the treatment of leishmaniasis, STFC ISIS Neutron and Muon Source" (2022), https://doi.org/10.5286/ISIS.E.RB2210097.

[37] "Mantid (2013): Manipulation and Analysis Toolkit for Instrument Data.; Mantid Project.http://dx.doi.org/10.5286/SOFTWARE/MANTID.".
[38] O. Arnold et al., Mantid—Data analysis and visualization package for neutron scattering and μ SR experiments, Nucl Instrum Methods Phys Res A 764 (2014) 156–166, https://doi.org/10.1016/j.nima.2014.07.029.
[39] G.D. Wignall, F.S. Bates, Absolute calibration of small-angle neutron scattering data, J Appl Crystallogr 20 (1) (Feb. 1987) 28–40, https://doi.org/10.1107/S0021889887087181.
[40] M. Doucet *et al.*, "SasView version 5.0.4," Apr. 2021, doi: 10.5281/ZENODO.4467703.
[41] J. Schwartz, E. Moreno, A. Calvo, L. Blanco, C. Fernández-Rubio, C. Sanmartín, P. Nguewa, J.M. Irache, E. Larrea, S. Espuelas, Combination of paromomycin plus human anti-TNF-α antibodies to control the local inflammatory response in BALB/ mice with cutaneous leishmaniasis lesions, J Dermatol Sci 92 (1) (2018) 78–88.
[42] J. Schindelin, I. Arganda-Carreras, E. Frise, V. Kaynig, M. Longair, T. Pietzsch, S. Preibisch, C. Rueden, S. Saalfeld, B. Schmid, J.-Y. Tinevez, D.J. White, V. Hartenstein, K. Eliceiri, P. Tomancak, A. Cardona, Fiji: An open-source platform for biological-image analysis, Nat. Methods 9 (7) (2012) 676–682.
[43] G. González-Gaitano, M.A. da Silva, A. Radulescu, C.A. Dreiss, Selective tuning of the self-assembly and gelation of a hydrophilic poloxamine by cyclodextrins, Langmuir 31 (20) (May 2015) 5645–5655, https://doi.org/10.1021/acs.langmuir.5b01081.
[44] R.M. Ziolek, J. Omar, W. Hu, L. Porcar, G. González-Gaitano, C.A. Dreiss, C.D. Lorenz, Understanding the pH-Directed Self-Assembly of a Four-Arm Block Copolymer, Macromolecules 53 (24) (2020) 11065–11076.
[45] A. Bahadur, S. Cabana-Montenegro, V.K. Aswal, E.V. Lage, I. Sandez-Macho, A. Concheiro, C. Alvarez-Lorenzo, P. Bahadur, NaCl-triggered self-assembly of hydrophilic poloxamine block copolymers, Int J Pharm 494 (1) (2015) 453–462.
[46] Y. Kadam, K. Singh, D.G. Marangoni, J.H. Ma, V.K. Aswal, P. Bahadur, Induced micellization and micellar transitions in aqueous solutions of non-linear block copolymer Tetronic® T904, J Colloid Interface Sci 351 (2) (Nov. 2010) 449–456, https://doi.org/10.1016/j.jcis.2010.07.046.
[47] N. James Chang and E. W. Kaler, "The Structure of Sodium Dodecyl Sulfate Micelles In Solutions of H20 and D20," 1985. [Online]. Available: https://pubs.acs.org/sharingguidelines.
[48] P. Mukerjee, P. Kapauan, and H. G. Meyer, "Micelle formation and hydrophobic bonding in deuterium oxide," *Journal of Physical Chemistry*, vol. 70, no. 3, 1966, doi: 10.1021/j100875a029.
[49] R. Serra-Gómez, C.A. Dreiss, J. González-Benito, G. González-Gaitano, Structure and rheology of poloxamine T1107 and its nanocomposite hydrogels with cyclodextrin-modified barium titanate nanoparticles, Langmuir 32 (25) (Jun. 2016) 6398–6408, https://doi.org/10.1021/acs.langmuir.6b01544.
[50] J. Puig-Rigall, I. Obregon-Gomez, P. Monreal-Pérez, A. Radulescu, M.J. Blanco-Prieto, C.A. Dreiss, G. González-Gaitano, Phase behaviour, micellar structure and linear rheology of tetrablock copolymer Tetronic 908, J Colloid Interface Sci 524 (2018) 42–51.
[51] J. Joseph, C.A. Dreiss, T. Cosgrove, J.S. Pedersen, Rupturing polymeric micelles with cyclodextrins, Langmuir 23 (2) (Jan. 2007) 460–466, https://doi.org/10.1021/la061850g.
[52] S. Manet, A. Lecchi, M. Impéror-Clerc, V. Zholobenko, D. Durand, C.L.P. Oliveira, J.S. Pedersen, I. Grillo, F. Meneau, C. Rochas, Structure of micelles of a nonionic block copolymer determined by SANS and SAXS, J. Phys. Chem. B 115 (39) (2011) 11318–11329.
[53] M. Rakotomanga, P.M. Loiseau, M. Saint-Pierre-Chazalet, "Hexadecylphosphocholine interaction with lipid monolayers", *Biochimica et Biophysica Acta (BBA)* -, Biomembranes 1661 (2) (2004) 212–218, https://doi.org/10.1016/j.bbamem.2004.01.010.
[54] M.B. Barioni, A.P. Ramos, M.E.D. Zaniquelli, A.U. Acuña, A.S. Ito, Miltefosine and BODIPY-labeled alkylphosphocholine with leishmanicidal activity: Aggregation properties and interaction with model membranes, Biophys Chem 196 (2015) 92–99, https://doi.org/10.1016/j.bpc.2014.10.002.
[55] C.H. Walker, The Hydrophobic Effect: Formation of Micelles and Biological Membranes, FEBS Lett 124 (1) (Feb. 1981) 127, https://doi.org/10.1016/0014-5793(81)80071-3.
[56] A. Rey-Rico, M. Silva, J. Couceiro, A. Concheiro, C. Alvarez-Lorenzo, Osteogenic efficiency of in situ gelling poloxamine systems with and without bone morphogenetic protein-2, Eur Cell Mater 21 (2011) 317–340, https://doi.org/10.22203/eCM.v021a24.
[57] M.F. Peralta, N.A. Usseglio, M.E. Bracamonte, M.L. Guzmán, M.E. Olivera, J.D. Marco, P.A. Barroso, D.C. Carrer, Efficacy of topical Miltefosine formulations in an experimental model of cutaneous leishmaniasis, Drug Deliv Transl Res 12 (1) (2022) 180–196.
[58] P. Escobar, S. Matu, C. Marques, S.L. Croft, Sensitivities of Leishmania species to hexadecylphosphocholine (miltefosine), ET-18-OCH3 (edelfosine) and amphotericin B, Acta Trop. 81 (2) (2002) 151–157.
[59] M.L. Cuestas, A. Sosnik, V.L. Mathet, Poloxamines display a multiple inhibitory activity of ATP-binding cassette (ABC) transporters in cancer cell lines, Mol Pharm 8 (4) (Aug. 2011) 1152–1164, https://doi.org/10.1021/mp2000132.
[60] C.C. Castronuovo, M.L. Cuestas, J.R. Oubiña, V.L. Mathet, Effect of several PEO-PPO amphiphiles on bax, bcl-2, and hTERT mRNAs: An insight into apoptosis and cell immortalization induced in hepatoma cells by these polymeric excipients, Biotechnol Appl Biochem 63 (2) (Mar. 2016) 273–280, https://doi.org/10.1002/bab.1352.
[61] V. Singh, K. Eljaaly, S. Md, N.A. Alhakamy, P. Kesharwani, Triblock copolymeric drug delivery as an emerging nanocarrier for treatment of infectious diseases, J. Drug Delivery Sci. Technol. 75 (2022) 103691.
[62] M.S.H. Akash, K. Rehman, Recent progress in biomedical applications of Pluronic (PF127): Pharmaceutical perspectives, J. Control. Release 209 (2015) 120–138.
[63] M.A. Firestone, A.C. Wolf, S. Seifert, Small-angle X-ray scattering study of the interaction of poly(ethylene oxide)-b-poly(propylene oxide)-b-poly(ethylene oxide) triblock copolymers with lipid bilayers, Biomacromolecules 4 (6) (Nov. 2003) 1539–1549, https://doi.org/10.1021/bm034134r.
[64] A. Pfalzgraff, S. Bárcena-Varela, L. Heinbockel, T. Gutsmann, K. Brandenburg, G. Martinez-de-Tejada, G. Weindl, Antimicrobial endotoxin-neutralizing peptides promote keratinocyte migration via P2X7 receptor activation and accelerate wound healing in vivo: Anti-endotoxin peptides promote wound healing, Br. J. Pharmacol. 175 (17) (2018) 3581–3593.